Catalysis Science & Technology

ROYAL SOCIETY OF CHEMISTRY

PAPER

View Article Online
View Journal

Cite this: DOI: 10.1039/d0cy00499e

CO activation and methanation mechanism on hexagonal close-packed Co catalysts: effect of functionals, carbon deposition and surface structure†

Hai-Yan Su, [a] Changlin Yu, [b] Jin-Xun Liu,[c] Yonghui Zhao,[d] Xiufang Ma,[e] Jie Luo,[c] Chenghua Sun, [a] Wei-Xue Li *[c] and Keju Sun*[f]

Received 12th March 2020,
Accepted 19th April 2020

DOI: 10.1039/d0cy00499e

rsc.li/catalysis

CO methanation is an industrially important reaction for the removal of trace amounts of CO from the hydrogen feed for ammonia production and in proton exchange membrane fuel cells. Although the H-assisted CO dissociation mechanism has been extensively elucidated, discrepancies exist in determining through which C_1-oxygenate intermediates the C–O bonds are broken. Using density functional theory calculations and microkinetic studies, we show that theoretical studies can reach agreement in C–O bond scission *via* the CHO intermediate on Co(0001) at a low coverage regime, and this mainly controls the CO methanation rate. This mechanism is independent of the functionals considered and the presence of graphitic carbon, and likely also pertains to other Co surface structures, including some open facets and step sites. The work provides fundamental insights into the mechanistic discrepancies relating to CO activation and methanation on hexagonal close-packed Co catalysts, which can potentially be used to design improved CO hydrogenation catalysts.

Introduction

The CO methanation reaction, namely $CO + 3H_2 \rightarrow CH_4 + H_2O$, is an industrially important reaction for the removal of trace amounts of CO from the hydrogen feed for ammonia production[1] and in proton exchange membrane fuel cells.[2] CO methanation is also used in connection with the gasification of coal[3] and Fischer–Tropsch synthesis.[4] A number of experimental[1,5–13] and theoretical works[14–23] have been conducted to elucidate the reaction mechanism, however several details regarding CO activation and methanation pathways remain of some debate, and this greatly hampers the design and development of the improved catalyst. The first step towards optimized catalyst performance is to understand the controversies, reach an agreement in the reaction mechanism and in turn identify the key factors that control the reaction activity at the atomic scale.

Both experimental[1,5–9] and theoretical studies[14–23] have elucidated a H-assisted CO dissociation mechanism on supported Ru, Co, Fe and Ni based catalysts and model surfaces. However, diverse C_1-oxygenate precursors and reaction pathways for C–O bond scission have only been speculated. For instance, CHO has been identified as the key intermediate for CO methanation on Ru/Al_2O_3 catalysts by *in situ* diffuse reflectance infrared Fourier transform spectroscopy and steady-state isotope transient kinetic analysis.[5] By combining H_2/D_2 isotope measurements and kinetic analysis on Co and Fe nanoparticles, as well as density functional theory (DFT) calculations on model Co(0001) and Fe(110) surfaces, Iglesia *et al.*[6] and Holmen *et al.*[7] suggest that C–O bond scission occurs *via* an alcohol intermediate, CHOH. However, most of the theoretical calculations show that aldehyde intermediates CHO[14–18] or CH_2O[19,20] are the precursors for C–O bond scission on the

[a] School of Chemical Engineering and Energy Technology, Dongguan University of Technology, Dongguan 523808, China
[b] School of Chemical Engineering, Guangdong University of Petrochemical Technology, Maoming 525000, China
[c] Department of Chemical Physics, School of Chemistry and Materials Science, University of Science and Technology of China, Hefei 230026, China. E-mail: wxli70@ustc.edu.cn
[d] CAS Key Laboratory of Low-Carbon Conversion Science and Engineering, Shanghai Advanced Research Institute, Chinese Academy of Science, Shanghai 201203, China
[e] Shenzhen Key Laboratory of Advanced Thin Films and Applications, College of Physics and Optoelectronic Engineering, Shenzhen University, Shenzhen 518060, China
[f] Key Laboratory of Applied Chemistry, College of Environmental and Chemical Engineering, Yanshan University, Qinhuangdao 066004, China. E-mail: kjsun@ysu.edu.cn

† Electronic supplementary information (ESI) available: Effects of ZPE corrections; adsorption energies, geometries and coverages of intermediates; energetics, geometries and rates for elementary reactions; effects of surface structures and functions on the energetics; effects of temperature on coverage and reaction order; and a description of the microkinetic model. See DOI: 10.1039/d0cy00499e

close-packed metal surfaces. In particular, for a given metal surface, such as Co(0001), discrepancies exist in theoretical studies regarding C–O bond scission *via* a CHO[14–16] or CH_2O[19,20] intermediate. The reasons for the discrepancies between the theoretical studies and between the theoretical and experimental studies need to be well understood in order to better design and develop improved catalysts.

Several factors that may lead to the diverse C_1-oxygenate precursors and C–O bond scission pathways have come to our attention: (1) the existing theoretical studies consider specific CO activation pathways *via* aldehyde or/and alcohol intermediates. To our knowledge, no studies including all the C_1-oxygenate intermediates and relevant reaction pathways are available. The lack of systematic investigations leaves open the possibility that other intermediates may be responsible for C–O bond scission. (2) It has been shown that functionals may have a significant effect on Fischer–Tropsch synthesis.[24] The previous CO methanation calculations generally employed the generalized gradient approximation with the PW91[25] or PBE[26] exchange–correlation functional, and these often overestimate the interaction of O with the transition metals. This may lead to a higher stability of the aldehyde intermediates compared with their alcohol isomers, since O is bonded to the surfaces in the former instead of in the latter. Thus, the effect of functionals, including a wider range of the descriptions of adsorbate–surface interactions from strong to weak, should be investigated.[27] (3) Carbon deposition[10,28] has been detected on the surfaces of transition metal-based catalysts during CO hydrogenation, but it is unclear yet whether the presence of coke changes the relative stability of aldehyde and alcohol intermediates. (4) Theoretical studies mainly focus on the close-packed surfaces of transition metals. However, the metal nanoparticles employed in the experiments contain other surface sites such as open surfaces and steps *etc.* A systematic investigation into how the relative stability of the aldehyde and alcohol intermediates depends on the surface structure is still missing.

In addition to the CO activation pathways, controversies also exist in the rate limiting step of CO methanation. Surface science experiments by de Groot *et al.* found equal apparent activation energy for methane formation on Co(0001) and Co(11–20).[10] They proposed a similar rate limiting step of CH_3 hydrogenation on the surfaces. However, by combining experimental and theoretical studies, Iglesia *et al.*[6,9] and Holmen *et al.*[7] proposed a CO hydrogenation pathway limited by H-assisted CO dissociation on the close-packed Co, Fe and Ru surfaces.

In order to provide insights into the mechanistic discrepancies, we systematically investigated all the C_1-oxygenate intermediates and relevant pathways for CO activation and methanation on Co(0001) using DFT calculations and microkinetic simulations. We also studied the effects of functionals, carbon deposition and surface structure on the CO methanation mechanism over hexagonal close-packed (HCP) Co catalysts. The strongly constrained and appropriately normed (SCAN) meta-GGA,[29] PBE[26] and Bayesian error estimation functionals with van der Waals correlation (BEEF-vdW),[30] which describes a wide range of adsorbate–surface interactions from strong to weak, were chosen to illustrate the effect of the functionals. The thermodynamically stable graphene configurations,[31–33] the open Co surfaces (0001, 10–10, 10–12, 11–20 and 10–11) that we previously identified on HCP Co catalysts[15] and stepped Co were used to investigate the effect of carbon deposition and the Co surface structure. Finally, we discuss the possible effect of support and adsorbate–adsorbate interactions in CO methanation. The work provides fundamental understanding into the mechanistic discrepancies in CO activation and methanation on HCP Co catalysts, and the insights obtained can be applied to other CO hydrogenation catalysts such as Ru, Fe and Ni based catalysts.

Methods

Spin-polarized DFT calculations were performed with the Vienna *ab initio* simulation package (VASP).[34] The interaction between the ionic cores and the electrons was described by the projector-augmented wave (PAW) method, and the Kohn–Sham valence electronic wavefunction was expanded in a plane-wave basis set with a kinetic energy cutoff of 400 eV. The exchange–correlation effects were represented within the generalized gradient approximation (GGA) using the PBE exchange–correlation functional,[26] unless otherwise indicated. The energies were converged to within 10^{-4} eV per atom, and the forces were converged to within 0.03 eV $Å^{-1}$.

The $p(2 \times 2)$ slab models were used for all the surfaces exposed in the morphology of the HCP Co particle (see our previous work[15] for more details), with the exception of Co(0001) with a (3×3) surface unit cell. The stepped Co was modeled using a (7×3) close-packed surface, in which three neighboring rows of metal atoms on the top layer were removed. All the surfaces were simulated by four equivalent (0001) layer slabs. Neighboring slabs were separated by a vacuum of at least 15 Å to avoid interactions between them. The surface Brillouin zone was sampled with a $(4 \times 4 \times 1)$, $(7 \times 4 \times 1)$, $(3 \times 7 \times 1)$, $(4 \times 4 \times 1)$, $(5 \times 5 \times 1)$ and $(4 \times 2 \times 1)$ Monkhorst–Pack *k*-points grid mesh for (0001), (10–10), (10–12), (11–20), (10–11) and stepped Co, respectively.[35] All the adsorbates and the topmost two equivalent (0001) layers were relaxed, and the remaining layers were fixed in their bulk positions. The lattice constants for hexagonal bulk cobalt were calculated to be $a = b = 2.50$ Å and $c = 4.03$ Å, which are in good agreement with the experimental values ($a = b = 2.51$ Å and $c = 4.06$ Å). The adsorption energy (ΔE_{ads}) was calculated using the most stable adsorption configurations (E_{total}) relative to the clean surfaces (E_{slab}) and the isolated adsorbates (E_{ad}):

$$\Delta E_{ads} = E_{total} - E_{slab} - E_{ad} \quad (1)$$

All transition states (TSs) were located by the force reversed method[36] and the climbing-image nudged elastic

band method (CI-NEB).[37] The relaxation was stopped until the residual forces in each atom were smaller than 0.03 eV Å^{-1}. The elementary activation barrier ΔE_{act} and reaction energy ΔH were calculated with respect to the most stable state for separate adsorption of adsorbates on the surfaces. For the C/Co system, ΔH was calculated with respect to the most stable state for the co-adsorption of adsorbates. We performed zero point energy (ZPE) corrections for several representative types of surface reactions involving C–H and O–H bond formation, and C–O bond scission (see Table S1†). The effect of ZPE corrections on the ΔE_{act} and ΔH is slight, with a change of 0.02–0.12 eV and 0.04–0.11 eV, and this would not change the activity trends of the surface reactions. Thus, ZPE corrections are not included in this work.

The formation heat (ΔH_f) for the C_1-oxygenate intermediates CH_xO in Fig. 5a are defined as the reaction free energies of the following reaction:[16]

$$CO(g) + 2H_2(g) + (5 - x)* \rightarrow CH_xO* + (4 - x)H* \quad (2)$$

where CO and H_2 are in the gas phase, CH_xO* and H* are the adsorbed species on the surfaces, and * indicates the vacant sites on the clean surfaces. H* is used because H_2 dissociation is exothermic and hydrogenation reactions occur *via* H* on Co(0001) under CO hydrogenation conditions. The ΔH_f values for the C_1-oxygenate intermediates are obtained by evaluating free-energy differences between the sub-systems involved in reaction (2), as follows:

$$\Delta H_f = G_{CH_xO*} + (4 - x)G_{H*} - G_{CO(g)} - 2G_{H_2(g)} - (5 - x)G* \quad (3)$$

where G is the free energy of each sub-system involved in reaction (2). We neglected the effect of entropy (S_m) for the adsorbed species, and only included that for the gas-phase species. For instance, the S_m value of a linear molecule was calculated as follows:

$$S_m = S_{mt} + S_{mr} \quad (4)$$

$$S_{mt} = R \ln [(2\pi m k_B T)^{3/2} k_B T/(h^3 P)] + 5/2R \quad (5)$$

$$S_{mr} = R \ln (T/\theta_{rot}) + R \quad (6)$$

where S_{mt} and S_{mr} are the translational and rotational entropies, respectively. R, m, k_B, T, h, P and θ_{rot} are the molar gas constant, molecular mass, Boltzmann constant, absolute temperature, Planck constant, partial pressure and characteristic rotation temperature for the gaseous molecule, respectively. 500 K, 1 atm and H_2/CO ratio of 2 were employed in the calculations for ΔH_f and ΔG in Fig. 3.

Results and discussion

CO methanation mechanism on Co(0001)

In general, CO methanation on Co(0001) starts with a H-assisted CO activation *via* the aldehyde species CH_xO or alcohol species $CH_{x-1}OH$ (x = 1–3), which undergo C–O bond scission to $CH_x(CH_{x-1})$, followed by sequential hydrogenation to CH_4. The O or OH produced can eventually be removed by H_2O or CO_2. To provide a complete analysis of the CO methanation mechanism, we not only investigated all the C_1-oxygenate intermediates and relevant pathways for C–O bond scission, but also various possible pathways for H_2O formation, by either H + OH or OH + OH, and CO_2 formation by either CO + O or dehydrogenation of COOH/HCOO, produced by CO + OH/CHO + O.

We first studied the adsorption of various species involved in CO methanation on Co(0001). The adsorption energies, ΔE_{ads}, and the most favorable adsorption geometries are shown in Table S2† and Fig. 1. The adsorption of the species such as CO, CH_x (x = 0–3) and H on Co(0001) have been described in detail in our previous work.[14–16] In the present work, we mainly concentrate on the C_1-oxygenate intermediates.

As shown in Fig. 1a, COH binds through its C atom to a hcp site with a ΔE_{ads} value of −4.27 eV, which is in excellent agreement with that of a previous DFT study.[21] CHOH also binds through C to a hcp site (Fig. 1b); the ΔE_{ads} value is −2.94 eV. Hu *et al.* found similar adsorption geometry but a much larger ΔE_{ads} value of −3.82 eV.[21] Mavrikakis *et al.* reported a ΔE_{ads} value of −3.00 eV,[6] which is quasi degenerate to our value, but no structural information was provided to compare with our result. Our calculations show that the favorable bridge-hcp-bridge configurations for CHO and CH_2O adsorption (Fig. 1c and d), which agree well with those calculated by Inderwildi *et al.*,[19] are 0.09 and 0.08 eV more stable than the bridge-hcp-top configurations found by Saeys *et al.*[20] and Hu *et al.*[21] As shown in Fig. 1e and f, CH_3O and CH_2OH bind through O and C to the hcp and bridge sites, with the methyl hydrogen and hydroxyl hydrogen located at the fcc and bridge sites, respectively, and these slightly differ from the top site preference for the H atoms in previous calculations.[21] The slight structural difference causes marginal variation in ΔE_{ads}. For instance, our calculations show that the structure of CH_3O in Fig. 1e is slightly more stable than that in previous work by 0.04 eV.[21] The discrepancies in the energetic and structures for C_1-oxygenate intermediate adsorption between our results and previous DFT calculations[19–21] also lead to varied transition state (TS)

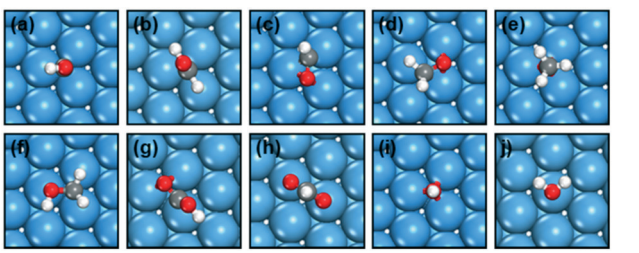

Fig. 1 Optimized configurations for (a) COH, (b) CHOH, (c) CHO, (d) CH_2O, (e) CH_3O, (f) CH_2OH, (g) COOH, (h) HCOO, (i) OH and (j) H_2O adsorption on Co(0001). The blue, grey, red and white balls represent Co, C, O and H atoms, respectively.

structures, activation energies ΔE_{act} and H-assisted CO activation pathways accordingly, as we will discuss below. In addition, we also investigated the adsorption of COOH and HCOO, which are related to CO_2 formation. COOH prefers to bind through both C and O (denoted "C_{top}-hcp-O_{bri}" in Fig. 1g), with the O–H bond pointing towards the surface and a ΔE_{ads} value of −2.24 eV. HCOO prefers a bidentate structure (Fig. 1h) with a ΔE_{ads} value of −3.06 eV. Adsorbed COOH and HCOO states are isomers of each other, where HCOO is thermodynamically more stable on Co(0001) by 0.43 eV.

The thermochemistry and ΔE_{act} for all the elementary steps have been systematically studied, and are listed in Table S3,† and the structures at the TSs are shown in Fig. 2. Since CO dissociation and CH_x (x = 0–3) hydrogenation on Co(0001) have been extensively discussed in our previous work,[14–16,22] we only describe the elementary steps involving the H-assisted CO activation and H_2O and CO_2 formation below.

Although CHO formation (ΔH = 1.08 eV) is thermodynamically less favorable than COH formation (ΔH = 0.85 eV) from CO hydrogenation, the close proximity of C to the Co(0001) surface in adsorbed CO results in more facile hydrogenation through C (ΔE_{act} = 1.23 eV) than through O (ΔE_{act} = 1.85 eV). Our calculated ΔH and ΔE_{act} values agree well with the previous study.[21] Once CHO is formed on the surface, it can undergo C–O bond scission or it can hydrogenate to the C or O end, leading to the formation of CH_2O or CHOH, respectively. We show that C–O bond scission in CHO has a ΔE_{act} value of 0.68 eV, which is much lower than the values of 1.00 and 0.93 eV calculated by Inderwildi *et al.*[19] and Saeys *et al.*[20] The discrepancy between our result and that of a previous theoretical study by Saeys *et al.* can be explained by the different structures at the initial states and TSs. As discussed above, the bridge-hcp-bridge configuration (Fig. 1c) we used for CHO adsorption is slightly more stable than the bridge-hcp-top configuration found by Saeys *et al.* Moreover, we found that O binds at the hcp site, and CH binds at the adjacent bridge site at the TS (insert in Fig. 3), in contrast with both fragments at the bridge sites in the DFT calculations by Saeys *et al.* In addition, Inderwildi *et al.* only provides the structure for CHO adsorption, which agrees well with our work, yet the lack of the TS structure precludes the understanding of the ΔE_{act} difference. In the case of CHO hydrogenation, we show that CH_2O formation is more favorable than CHOH formation both thermodynamically (0.23 *vs.* 0.43 eV) and kinetically (0.45 *vs.* 1.17 eV), and this is in excellent agreement with the previous DFT study.[21]

The CH_2O produced can undergo C–O bond scission or it can hydrogenate to the C or O end, leading to the formation of CH_3O or CH_2OH, respectively. The ΔE_{act} value we calculated for CH_2O decomposition was 0.70 eV, which is equal to the value in a previous study by Saeys *et al.*[20] However, both our ΔE_{act} values are lower than those reported by Inderwildi *et al.*[19] and Hu *et al.*,[21] with corresponding values of 0.85 and 0.95 eV. The TS structures in our study (insert in Fig. 3) and in previous DFT studies by Saeys *et al.* are almost the same, with the H atoms located at the hcp and top sites, respectively, slightly differing from the study by Hu *et al.* with both H atoms located at the hcp sites. In addition, the discrepancy in ΔE_{act} may also arise from the different methods used (VASP *vs.* SIESTA). Compared to CH_2-OH, CH_3O is preferred to be produced from CH_2O hydrogenation thermodynamically (0.46 *vs.* −0.38 eV) and kinetically (1.07 *vs.* 0.58 eV), and this agrees qualitatively with the previous theoretical study by Hu *et al.*[21] However, the high ΔE_{act} value for CH_2OH formation and CH_3O decomposition (1.38 eV) exclude both intermediates as possible precursors for C–O bond scission.

Once the C–O bond is broken *via* aldehyde or alcohol intermediates, the O or OH produced can be removed from the surface by H_2O or CO_2. There are two possible pathways for H_2O formation on Co (0001): (i) by hydrogenation of OH, with a relatively high ΔE_{act} value of 1.49 eV and a ΔH value of 0.60 eV, formed by either C–O bond scission in the alcohol intermediates or by O hydrogenation, and this is endothermic by 0.28 eV with a ΔE_{act} value of 1.22 eV, and (ii) by the facile H-transfer process from one OH to another; the step is endothermic by 0.32 eV, with a ΔE_{act} value of 0.57 eV (see the TS structures in Fig. 2j–l). Compared to H_2O formation, CO_2 formation is more complicated. We considered three possible pathways: (i) CO oxidation with atomic O, which is highly endothermic by 1.03 eV with a large ΔE_{act} value of 1.37 eV, (ii) by CO oxidation with OH, to form the COOH species. Similar to CO + O, this step is also highly endothermic (ΔH = 0.94 eV) and has a large ΔE_{act} value of 1.31 eV. The COOH formed may subsequently decompose to give CO_2 and H. The step is exothermic by 0.19 eV, and has a large ΔE_{act} value of 1.00 eV. We also considered COOH + OH → CO_2 + H_2O, but due to the unfavorable thermochemistry (ΔH = 0.40 eV) compared to that of COOH → CO_2 + H and the lack of OH under real CO methanation conditions (see Table S2†), we did not expand on the details of that elementary step here, and (iii) CHO oxidation with O to form a HCOO species. This step is

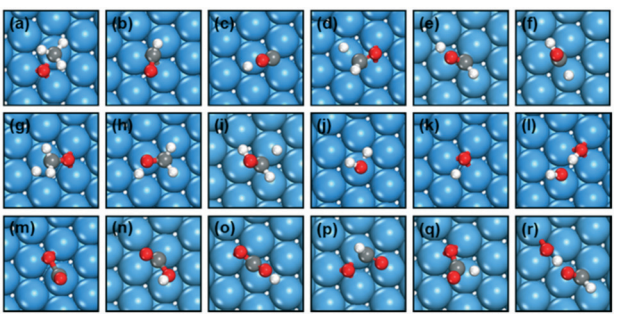

Fig. 2 Optimized configurations at the transition states of (a) CH_3O → CH_3 + O, (b) CO + H → CHO, (c) CO + H → COH, (d) CHO + H → CH_2O, (e) CHO + H → CHOH, (f) COH + H → CHOH, (g) CH_2O + H → CH_3O, (h) CH_2O + H → CH_2OH, (i) CHOH + H → CH_2OH, (j) OH + H → H_2O, (k) O + H → OH, (l) 2OH → H_2O + O, (m) CO + O → CO_2, (n) CO + OH → COOH, (o) COOH → CO_2 + H, (p) CHO + O → HCOO, (q) HCOO → CO_2 + H and (r) CHO + OH → CHOH + O on Co(0001).

exothermic by 0.29 eV, with a ΔE_{act} value of 0.66 eV. The HCOO species may then decompose to yield CO_2, with ΔH and ΔE_{act} values of 0.24 and 0.94 eV, respectively. The TS structures for CO_2 formation can be found in Fig. 2m–q.

The minimum energy paths for CO methanation are represented by a one-dimensional potential energy surface diagram in Fig. 3. Among all the C_1-oxygenate intermediates of CH_xO and $CH_{x-1}OH$ (x = 1–3), CHO is the most preferred for C–O bond scission, followed by CH_2O, as shown in Fig. 3 and Table S3.† This seems to contradict the mechanism presented by Inderwildi *et al.*[19] and by Saeys *et al.*,[20] where C–O bond scission *via* CH_2O was more favorable than *via* CHO. However, the discrepancies can be explained by the lower ΔE_{act} we found for CHO decomposition, leading to the switch to the favorable C–O bond scission pathway. By systematic investigations of the reaction pathways involving all the C_1-oxygenate intermediates, and comparison of the energetic and structural information with previous DFT calculations,[19–21] we revealed the reason for the discrepancies in the H-assisted CO activation mechanism on Co(0001) in the low coverage region.

Based on the DFT calculated energy profiles, a microkinetic simulation was conducted at typical CO hydrogenation conditions (483–573 K, 1 bar, H_2/CO = 2). A detailed description of the microkinetic model was given in our previous work[38] and in the ESI.† As listed in Table S3,† the direct CO dissociation is 8 orders of magnitude slower than the H-assisted CO dissociation (*via* CHO), and this is due to the high CO dissociation barrier (2.35 eV). This indicates that the H-assisted CO dissociation mechanism is dominant, and this is in excellent agreement with the previous experimental study, which shows a strong increase in the dissociation rate of adsorbed CO upon exposure to hydrogen on cobalt nanoparticles.[8] Among the H-assisted CO dissociation pathways, C–O bond scission *via* the CO → CHO → CH + O pathway has the highest net rate, followed by the CO → CHO → CH_2O → CH_2 + O pathway, suggesting that CHO is a key intermediate in the H-assisted CO activation mechanism. These results agree well with the *in situ* diffuse reflectance infrared Fourier transform spectroscopy and steady-state isotope transient kinetic experiments, where CHO has been identified as the key intermediate for CO methanation on Ru/Al_2O_3 catalysts.[5] Nevertheless, the present H-assisted CO activation mechanism does not agree with that of previous DFT calculations *via* the CH_2O intermediate[19,20] and experimental studies *via* the CHOH intermediate.[6,7] The discrepancies with the theoretical studies have been assigned to the lower energy pathway we determined for CHO decomposition, and those with experiments will be addressed in the next sections.

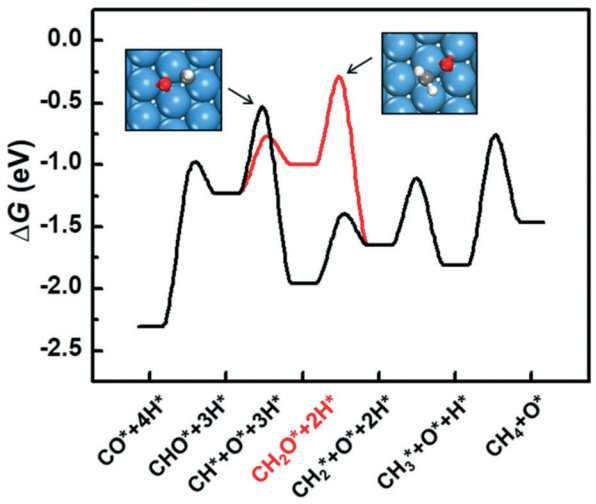

Fig. 3 The free energy profile of CO methanation on Co(0001) at 500 K, 1 atm and H_2/CO = 2. The reference zero of the Y axis corresponds to the energy of gaseous CO and H_2. Insert: The transition state configurations for CH_xO (x = 1, 2) decomposition.

The steady-state surface coverages on Co(0001) are given in Table S2 and Fig. S1a.† The surface is dominantly covered with CO at low temperatures due to strong CO adsorption. As the temperature increases, the coverage of CO gradually deceases, and this is accompanied by the increase of H coverage. At high temperatures, the coverage of H exceeds the coverage of CO, and the concentration of the empty sites also increases. Our calculated coverage agrees reasonably with the steady-state isotope transient kinetic experiments on the Co particles.[39]

It is not possible to compare reaction rates with experimental data at the present accuracy of the DFT-calculated barriers. The calculated rates are generally much lower than the experimental values for two reasons. Firstly, the calculated adsorption energies are often overestimated by PBE. Secondly, lateral interactions are not included. However, the present model is consistent with the preferential formation of H_2O instead of CO_2 in the products, as observed on the supported Co catalysts experimentally.[6] Fig. 4a shows the formation rate of CH_4, H_2O and CO_2 as a function of temperature. The microkinetic modeling indicates that, regardless of the temperature, O is removed preferentially by H_2O, and this is carried out by O hydrogenation to OH and subsequent OH disproportionation. The CO_2 formation, with the dominant pathway of CO + O (Table S3†), is inhibited by the high ΔE_{act} value of 1.37 eV.

The temperature dependence of the reaction orders of CO and H_2 is given in Fig. S1b.† Our simulations predict a negative CO reaction order at low temperatures (≤553 K) because the high CO coverage blocks the active sites. With increasing temperature, the CO reaction order becomes less negative. At higher temperatures (≥563 K), the CO coverage is greatly reduced, and the CO reaction order becomes positive. The reaction order with respect to H_2 was almost always positive at the temperatures studied. The negative reaction order for CO and the positive reaction order for H_2 agree well with previous experimental literature results on supported Co catalysts.[6]

The analysis of the degree of rate control (DRC) was performed to understand the importance of every elementary

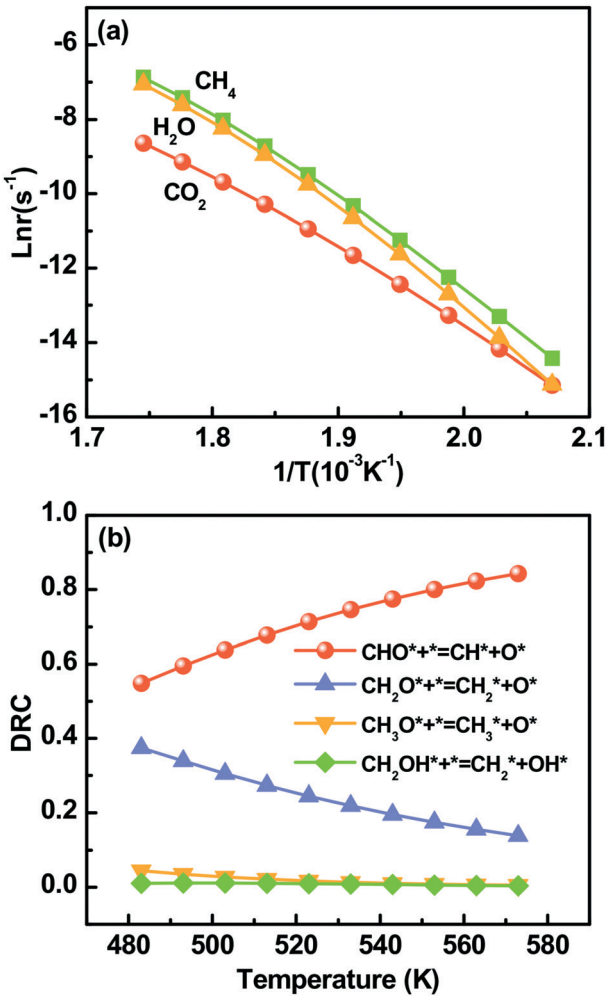

Fig. 4 (a) The reaction rate of product formation and (b) the degree of rate control (DRC) of the elementary steps for CO methanation as a function of temperature on Co(0001) *via* microkinetic modeling.

step to the total activity.[40] A positive value of DRC for a particular step means that this step is a rate limiting step, and that a decrease in the ΔE_{act} would increase the overall rate. A negative value indicates the opposite, and such steps are termed inhibition steps. Lowering the barriers of such steps decreases the overall rate. Fig. 4b clearly shows that, regardless of the temperature, the activity is mostly determined by CHO decomposition. This can be attributed to the low coverage of CHO on Co(0001), caused by the unfavorable thermochemistry of its formation (ΔH = 1.08 eV). In addition, CH_2O decomposition is also important to control the CO methanation activity on Co(0001) at the temperatures considered. Likewise, this step is relevant because of the endothermic CH_2O formation leading to its low coverage.

Combining DFT calculations and the microkinetic simulation enables comparison of the relative rate of the competing pathways and in turn identifies the energetically favorable pathways and intermediates. Nevertheless, locating the TSs for all the elementary reactions is still a demanding task, particularly when dealing with complicated reactions involving a large number of intermediates and elementary steps. We previously simplified this question by the use of more affordable descriptors, namely the formation heat ΔH_f and ΔE_{act} of C–O bond scission, to identify the key C_2-oxygenate intermediates in the CO insertion chain growth mechanism in Fischer–Tropsch synthesis.[16] We applied these descriptors to identify the key C_1-oxygenate intermediates in CO methanation and then assessed their reliabilities using the microkinetic model below.

There are six possible C_1-oxygenate precursors for C–O bond scission, namely CH_xO and $CH_{x-1}OH$ (x = 1–3). To achieve high scission activity, the C_1-oxygenate species should be easily produced (ΔH_f as negative/large as possible) and easily decomposed (ΔE_{act} as low as possible). As illustrated in Fig. 5a, the C_1-oxygenate species can be divided into three regions. CH_xOH (x = 1, 2) falls in region I with smaller ΔH_f values (−0.54 and −0.74 eV), indicating that it is difficult to form the species. On the other hand, although

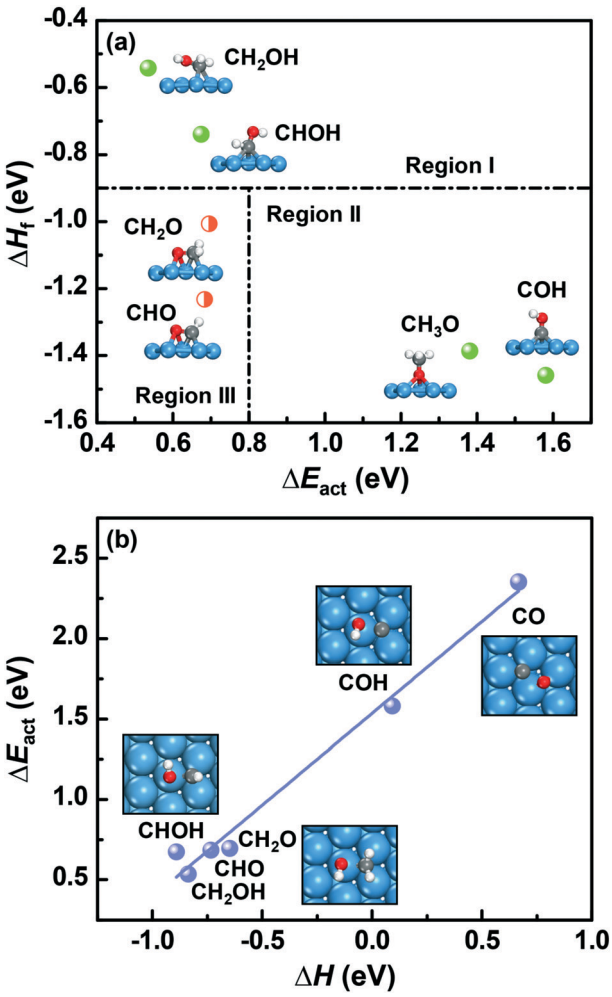

Fig. 5 (a) Formation heat ΔH_f of the C_1-oxygenate species as a function of the activation energy, ΔE_{act}, for C–O bond scission, and (b) the relation between ΔE_{act} and the reaction energy ΔH for C–O bond scission on Co(0001). Insert: Structures for (a) C_1-oxygenate species adsorption, and (b) transition states of C–O bond scission.

COH and CH_3O have large ΔH_f values (−1.39 and −1.46 eV), the high ΔE_{act} value (>1.3 eV, see region II) hinders their decomposition. CH_xO (x = 1, 2) that have large ΔH_f values (−1.01 and −1.23 eV) and a low ΔE_{act} value (<0.8 eV) in region III, however, are identified as the key precursors for the C–O bond scission in CO methanation. These results agree well with the above microkinetic studies, suggesting that the simple descriptors are effective in identifying the key intermediates and can simplify the reaction path study particularly for complex catalytic reactions. Finally, a linear Brønsted–Evans–Polanyi (BEP)-type relation[41] was found between ΔE_{act} and the reaction energy ΔH for the decomposition of the C_1-oxygenate intermediates, as shown in Fig. 5b, suggesting that the reaction kinetics and thermodynamics are well correlated in this case.

Effect of functionals

Having explained the discrepancy of the H-assisted CO dissociation mechanism in theoretical studies (*via* CHO *vs.* CH_2O), we turned to addressing this between theoretical and experimental studies (*via* aldehyde CHO/CH_2O *vs.* alcohol CHOH). As mentioned in the Introduction, the commonly used PW91[25] or PBE[26] exchange–correlation functional in CO methanation often overestimates the interaction of O with transition metals. This may result in the higher stability of aldehyde intermediates than their alcohol isomers, since O is bonded to the surfaces in the former rather than in the latter. Therefore, SCAN meta-GGA[29] and BEEF-vdW[30] that typically represent strong and weak bound limits were chosen to investigate the relative stability of the C_1-oxygenate intermediates on Co(0001), and these are compared with the PBE-based data. For simplification, we applied the lattice constant calculated by PBE to all the functionals, with the structures fully optimized for intermediate adsorption and surface reactions.

Fig. 6a shows how the total energy difference, ΔE, between the CH_xOH and $CH_{x+1}O$ (x = 0–2) isomers on Co(0001) vary with the functionals (see Fig. S2† for the adsorption energies of the species). A positive (negative) ΔE value represents a higher stability of $CH_{x+1}O$ (CH_xOH). For CH_xOH and $CH_{x+1}O$ (x = 1, 2) isomers, all the functionals predict higher stability of the latter. This indicates that the CHOH intermediate, as identified experimentally for C–O bond scission on Co particles, is less stable than its isomer CH_2O regardless of the functionals studied; SCAN and BEEF-vdW predict larger ΔE values than PBE. Compared to CH_xOH and $CH_{x+1}O$ (x = 1, 2), the case for COH and CHO isomers is slightly more elaborate. PBE and BEEF-vdW predict COH to be energetically favorable, while SCAN shows a higher stability of CHO. The qualitative disagreement between the predicted functionals results may originate from the similar stability of the two intermediates. These results suggest that the functionals are not responsible for the switch in the relative stability of the aldehyde and alcohol intermediates between the theoretical and experimental studies.

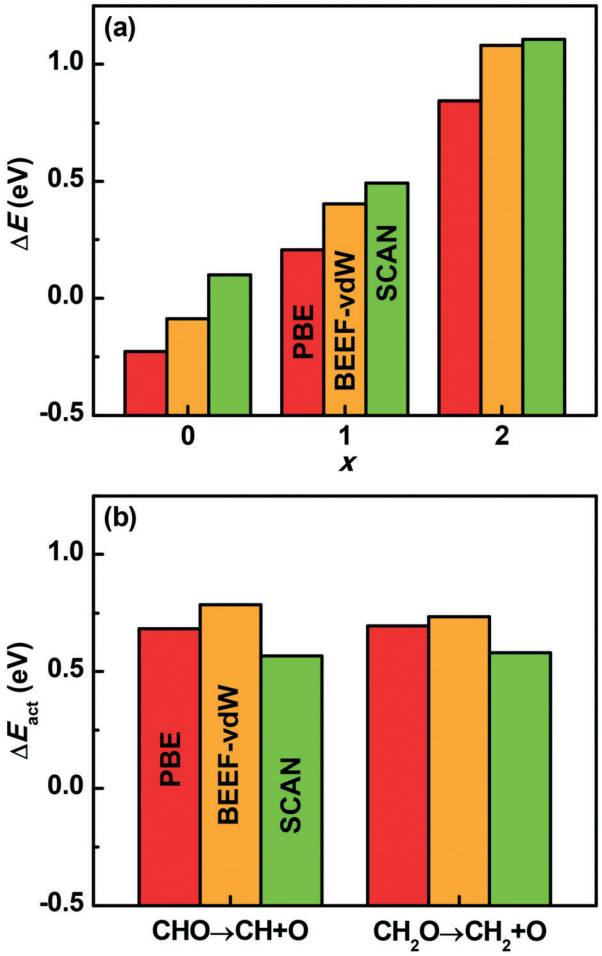

Fig. 6 The dependence of (a) the total energy difference, ΔE, between alcohol intermediates, CH_xOH, and their aldehyde isomers, $CH_{x+1}O$ (x = 0–2), and (b) the activation energy, ΔE_{act}, of C–O bond scission in CH_xO (x = 1, 2) on the functionals over Co(0001).

Apart from the thermodynamic stability of the C_1-oxygenate intermediates, we also studied the effect of functionals on C–O bond scission in CH_xO (x = 1, 2). As shown in Fig. 6b, the ΔE_{act} value for CH_xO decomposition does not show a strong dependence on the functionals considered. The functional induced ΔE_{act} value differences for CHO and CH_2O decomposition are 0.22 eV and 0.15 eV at most; compared to PBE, BEEF-vdW predicts a higher ΔE_{act} value, whereas SCAN predicts a lower ΔE_{act} value. In addition, the functionals have a slight effect on the relative magnitude of ΔE_{act} between CHO and CH_2O decomposition. These results indicate that the selection of functionals will not alter the H-assisted CO dissociation pathway, that is, through the CHO intermediate.

Effect of carbon deposition

A carbonaceous layer, formed as a product of CO dissociation, has been detected on the transition metal-based catalyst surfaces during CO hydrogenation conditions.[10,28] It has been demonstrated that the carbon deposited can either

modify the behavior of the neighboring metal sites or act as active sites for some surface reactions. Despite numerous studies, to our knowledge no computational studies of how the presence of coke affects the relative stability of the CH_xO and $CH_{x-1}OH$ intermediates and the H-assisted CO dissociation pathways exist.

The graphitic carbon, which has been shown to be more stable than the carbidic carbon on the Co catalysts,[33] was chosen to simulate the carbon deposition in the present work. One six-membered ring and three six-membered rings (denoted by C_6 and C_{13}) of carbon atoms on the (4 × 4) Co(0001) surface were used to simulate different sizes of carbon fragments on the Co catalyst. As shown in Fig. 7a–d, there are four different C_6 arrangements, with the center at the top, fcc, hcp and bridge sites of Co (denoted by C_6-t, C_6-f, C_6-h and C_6-b), respectively. To compare the relative stability of the four coke configurations, we defined the average adsorption energy per carbon atom (ΔE_C) as follows:

$$\Delta E_C = (E_{total} - E_{slab} - N \times E_C)/N \quad (7)$$

where E_{total}, E_{slab} and E_c are the energies of the relaxed C/Co system, the clean Co surface and the carbon atom in the gas phase, respectively. N indicates the number of carbon atoms. The larger/more negative the ΔE_C value is, the more stable the coke configuration is. Fig. 8 indicates that C_6-t is energetically the most favorable, with a ΔE_C value of −7.13 eV. The remaining C_6-f, C_6-h and C_6-b configurations have quasi-degenerate ΔE_C values from −6.75 to −6.79 eV. Similarly, there are three stable C_{13} arrangements, with the center of the six-membered ring at the top, fcc and hcp sites of Co (denoted by C_{13}-t, C_{13}-f and C_{13}-h, see Fig. 7e–g), respectively. Following the C_6 configurations, C_{13}-t, with a ΔE_C value of −7.27 eV, is more stable than C_{13}-f and C_{13}-h by 0.05 and 0.19 eV (see Fig. 8). We then chose the C_6-t and C_{13}-t configurations (Fig. 7a and e) to model different sizes of carbon fragments on Co(0001), and studied the effect of the carbonaceous layer on the thermochemistry of the formation of the C_1-oxygenate intermediates, as shown below.

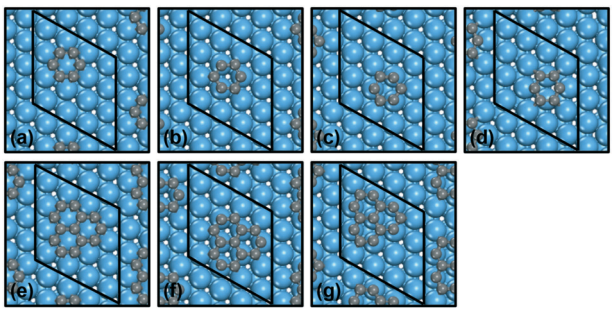

Fig. 7 Optimized configurations for C_6 with the center at (a) top, (b) fcc, (c) hcp, and (d) bridge sites (denoted by C_6-t, C_6-f, C_6-h and C_6-b, respectively), and C_{13} with the center at (e) top, (f) fcc and (g) hcp sites (denoted by C_{13}-t, C_{13}-f, and C_{13}-h) on (4 × 4) Co(0001). The blue and grey balls represent Co and C atoms, respectively.

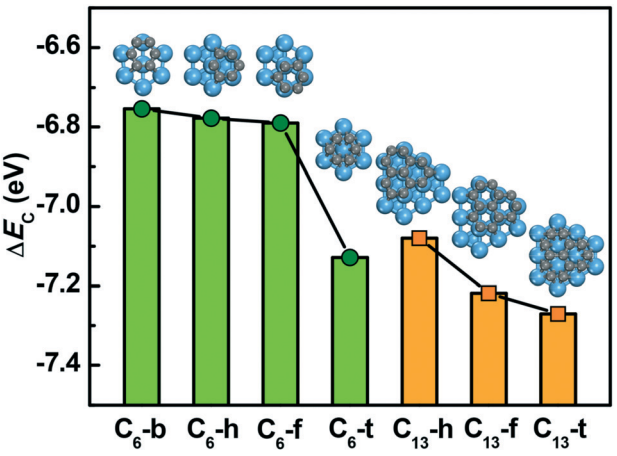

Fig. 8 The average adsorption energy per C atom, ΔE_C, of various C/Co(0001) models. Insert: The configurations of the C/Co(0001) models.

As expected, the C_1-oxygenate intermediates adsorb at the Co sites, and the C_6-t configuration only provides the active sites for atomic hydrogen adsorption, denoted by C_6-t_1 and C_6-t_2 in the insert of Fig. 9, where hydrogen points towards the fcc or hcp sites of Co, respectively. C_6-t_1 and C_6-t_2 have hydrogen adsorption energies of −0.97 and −1.02 eV, respectively; both bind hydrogen much stronger than Co(0001) by about 0.50 eV, as shown in Fig. 9. This leads to more difficult hydrogenation reactions than on Co. Compared with Co(0001), which has ΔH values of 1.08 and 0.85 eV for CO hydrogenation to CHO and COH, respectively, the presence of C_6-t makes both elementary steps more endothermic by 0.63 eV. Similarly, CH_2O and CHOH formation from CHO hydrogenation are also suppressed by the C_6-t layer, with ΔH values of 0.66 and 0.77 eV, respectively, in contrast with the corresponding values of 0.23 and 0.43 eV on Co(0001). In addition to C_6-t, we studied H

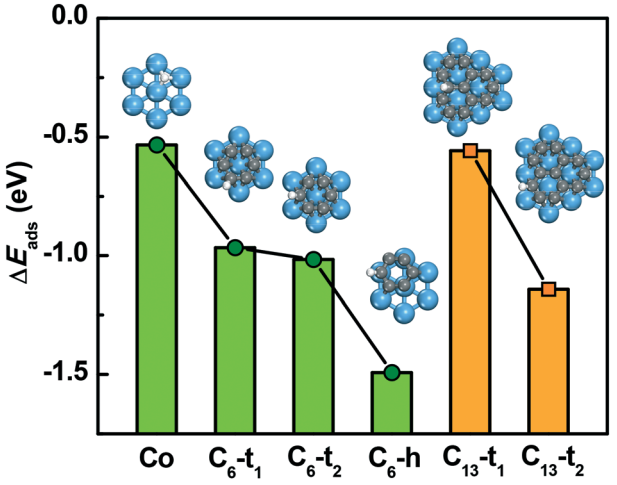

Fig. 9 The adsorption energy, ΔE_{ads}, of hydrogen (configurations in the insert) on Co(0001) and various C/Co(0001) models.

adsorption on the less stable C_6-h. As shown in Fig. 9, the H atom on C_6-h has a ΔE_{ads} value of −1.49 eV, which is much larger than that on C_6-t by about 0.50 eV. This can be understood well, as the C atom in C_6-h is less stabilized (smaller ΔE_C in Fig. 8) than in C_6-t, thereby leading to stronger binding with H and in turn less favorable formation of the C_1-oxygenate intermediates.

The above results suggest that the presence of the graphitic C_6 configurations on Co(0001) will be less favorable for hydrogenation reactions and for C_1-oxygenate intermediate formation. We note that in all the C_6 configurations, each C atom sits at the edge sites, coordinating with two adjacent C atoms, and this may be responsible for the strong H adsorption. In the C_{13}-t configuration, C sits not only at the edge sites, but also inside the carbonaceous layer, coordinating with three adjacent C atoms, and this may weaken H binding. Fig. 9 shows two representative adsorption sites for H adsorption on C_{13}-t, namely the C atoms coordinating with three (C_{13}-t_1) or two (C_{13}-t_2) adjacent C atoms. Compared to C_{13}-t_2, C_{13}-t_1 binds H more weakly, with the ΔE_{ads} value quasi-degenerate to that on Co(0001) (−0.56 *vs.* −0.53 eV). Although the weak H–C bond in C_{13}-t_1 will facilitate the hydrogenation reactions and the formation of the C_1-oxygenate intermediates thermodynamically, the unfavorable H location makes them kinetically unfeasible. Compared to C_{13}-t_2, the H on the C_{13}-t_1 site is in between two edge carbon atoms, possibly leading to strong steric repulsion at the TSs. Therefore, the present work indicates that the hydrogenation reactions involved in the H-assisted CO dissociation mechanism will prefer to happen at metallic Co without the participation of graphitic carbon.

Effect of surface structure

To date, theoretical investigations of CO dissociation and methanation pathways on Co catalysts have mainly focused on the close-packed Co(0001) surface. However, under realistic conditions, the Co nanoparticles employed in the experiments also contain other surface sites such as open surfaces and step sites *etc.* It is therefore essential to understand how the surface structure affects the stability of the C_1-oxygenate intermediates, particularly the relative stability of alcohol and aldehyde intermediates, and the CO activation and methanation pathways. We previously determined the equilibrium morphology of HCP Co particles that consist of (0001), (10–10), (11–20), (10–12) and (10–11) facets, with the ratio of 18%, 28%, 6%, 12% and 35%, respectively.[15] In this section, we chose CHOH and CH_2O intermediates as representative alcohol and aldehyde intermediates, to systematically study their relative stability on the Co facets exposed. In addition, the stepped site was also considered as a common defect site on the Co nanoparticles.

As shown in Fig. 10, the total energy difference, ΔE, between the CHOH and CH_2O intermediates is plotted as Co

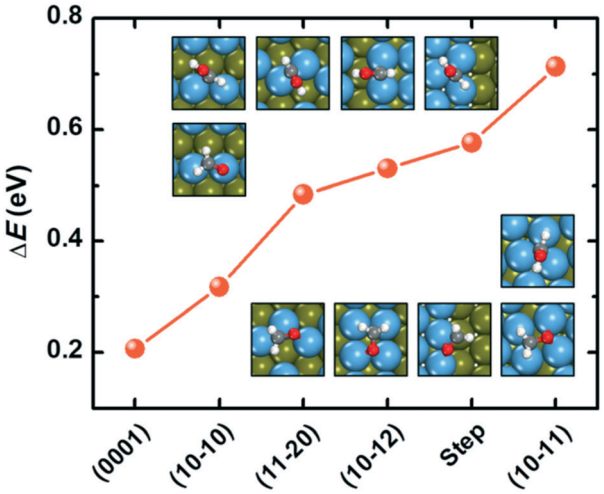

Fig. 10 The total energy difference, ΔE, between the CHOH and CH_2O intermediates as a function of the Co surface structure. Insert: Optimized configurations for CHOH (upper panel) and CH_2O (lower panel) adsorption on various Co facets. The blue, dark green, grey, red and white balls represent Co on the surface and subsurface, C, O and H atoms, respectively.

surface structures (see Table S4† for more details). A positive ΔE suggests that CH_2O is more stable, whereas a negative ΔE suggests CHOH to be more stable on the Co surfaces. It was found that ΔE was positive regardless of Co surface structure, indicating a higher stability of CH_2O than CHOH on all the Co surface sites considered. Co(0001) has a ΔE value of 0.21 eV, which is smaller than that of other Co surfaces and the step site, where ΔE falls in the region of 0.32–0.71 eV. Therefore, compared to Co(0001), the possibility for the H-assisted CO dissociation pathway *via* the CHOH intermediate is lower on the open Co surfaces and stepped Co from the point of view of thermochemistry.

We previously studied direct and H-assisted CO dissociation *via* CHO on various open Co surfaces and on the stepped site.[14–16] It was found that the CO dissociation mechanism is highly structure sensitive. On the active Co(11–21) and Co(10–11) surfaces, the direct routes have much lower barriers than the H-assisted routes by 0.59 and 0.23 eV, respectively, implying that the direct routes are preferable. The Co(10–12), stepped Co and Co(11–20) surfaces, with moderate activities, have similar barriers for the direct (1.39, 1.37 and 1.34 eV) and H-assisted routes (1.29, 1.35 and 1.40 eV), suggesting that both routes may contribute to CO dissociation. On the close-packed Co(0001) structure studied in this paper, the H-assisted route *via* the CHO intermediate is dominant.

Role of the oxide support

As discussed above, the functionals, carbon deposition and surface structures do not account for the discrepancy of the H-assisted CO dissociation pathways (*via* CHO *vs.* CHOH) between the present results and other experimental

findings[6,7] on Co catalysts. This urges us to reconsider if there are other low energy pathways for CHOH formation beyond the present investigations. Interestingly, we found a low ΔE_{act} value of 0.51 eV for the CHO* + OH* → CHOH* + O* pathway (see Fig. 2r for the TS structure), but because of the lower coverage of OH* than the vacant sites (θ_*/θ_{OH*} = 1.9 × 10^3–9.6 × 10^3) predicted by our microkinetic study, the rate of this step is lower than that of CHO* + * → CH* + O* by 3.6 × 10^{-2}–3.7 × 10^{-3} times on Co(0001) at 483–573 K. As a result, the CHOH mediated H-assisted CO activation is less favorable than the CHO mediated pathway. The low OH* coverage possibly originates from the high ΔE_{act} of 1.22 eV for the O* + H* → OH* + * step on Co(0001). In fact, the difficult OH* formation by O* hydrogenation is also found on other transition metals such as Ru, Rh and Pt surfaces, with a ΔE_{act} value of ~1.00 eV.[42] However, the OH* concentration on oxide supported metal particles experimentally can be much higher than on pure metals. On the one hand, the oxide supports themselves contain plenty of OH*. On the other hand, H_2 heterolytic dissociation to H atoms on the metal sites and protons on the oxides at the metal/oxide interface has been widely identified,[43] and this can largely facilitate the formation of OH*.

It has been demonstrated that proton transfer from the oxide support to the metal sites can be quite facile.[44] As shown in route 1 of Scheme 1, when a proton transfers from OH* on the oxide support to atomic O* on the metal sites, the OH* concentration and hence the CHO* + OH* → CHOH* + O* reaction on the metal (route 2) may be enhanced. We then included the role of the support in increasing OH* concentration by reducing the forward barrier of the O* + H* → OH* + * step to 0.95 and 0.31 eV, respectively. For both cases, although OH* formation was enhanced, the CHO* + OH* → CHOH* + O* rate was not remarkably improved relative to CHO* + * → CH* + O* ($r_{CHO* + OH*}/r_{CHO* + *}$ = 5.3 × 10^{-2}–4.1 × 10^{-3}) at the temperatures considered. This may be due to the fact that OH* can react faster through the 2OH* → H_2O* + O* reaction on Co(0001) (2.7 × 10^{-7}–8.6 × 10^{-4}), compared to the CHO* + OH* → CHOH* + O* step (1.1 × 10^{-8}–3.3 × 10^{-6}) at the temperatures studied. In addition, the rate of the CO* + OH* → COOH* + * step exceeds that of the CHO* + OH* → CHOH* + O* step with increasing OH* coverage, and this also results in the low rate of the latter. Finally, direct proton transfer from OH* on the oxide support to CHO* on the metal sites (route 3 in Scheme 1), which would depend on the nature of the support and the interface structure of Co and the support, needs to be further investigated.

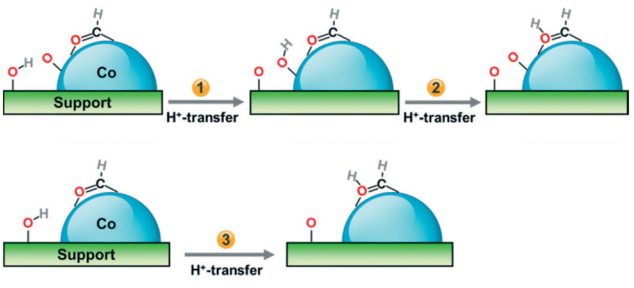

Scheme 1 A schematic diagram of the possible role of the oxide support in OH adsorption, proton transfer and CHOH formation.

Adsorbate–adsorbate interactions

In addition to the effect of the support, adsorbate–adsorbate interactions may also be responsible for the discrepancy in the H-assisted CO activation mechanism between the experimental findings[6,7] and the present work, where no such interactions are included. We previously employed a $(2\sqrt{3} \times 2\sqrt{3})$ $R30°$-CO structure (θ_{CO} = 7/12 ML) reported by low-energy electron diffraction and high-pressure infrared reflection absorption spectroscopy experiments,[45] to study the effect of co-adsorbates on CO activation and chain growth mechanism on Co(0001).[16] It was found that adsorption of CO and CH_x (x = 1, 2), which bind only through C, are weakened modestly by 0.37–0.47 eV with co-adsorbed CO. However, CHO binding through both C and O (which requires more sites on the surface), is weakened more by the co-adsorbed CO by 0.78 eV. This can be understood well in two respects: firstly, the molecules will share metal atoms with co-adsorbed CO at high coverages, giving rise to the substrate mediated repulsive interactions. Secondly, the steric hindrance contributes to additional repulsive interactions. With increasing molecule volume, the two repulsive interactions become more significant.

We also found that the co-adsorbed CO favors the bond-forming reactions as they release new active sites. For instance, CO + H → CHO is less endothermic by 0.15 eV with co-adsorbed CO. However, the bond-breaking reactions that require the creation of new active sites are largely inhibited at high coverages. In the presence of CO, the activation energy of CHO → CH + O is slightly increased by 0.04 eV. Thus, the total barrier for the two-step H-assisted CO dissociation, namely CO + H → CHO → CH + O, is decreased by 0.11 eV with co-adsorbed CO. The co-adsorbed CO could also affect the stability of other C_1-oxygenate intermediates and the barriers for their formation and decomposition.

In recent years, coverage effects have been considered in CO hydrogenation kinetics, and different coverage-dependent kinetic models including mean-field and extended phenomenological models have been developed.[46–49] However, it remains unclear if the interaction effects can alter the qualitative picture of mechanistic understanding. For example, Studt *et al.* found that the general trends in CO methanation activity on the transition metal surfaces are unchanged by the inclusion of interaction effects, and thus they suggest the use of the mean-field model without interaction effects for this reaction.[46] However, Hu *et al.* identified a H-assisted CO dissociation mechanism *via* CHOH on Co(0001) using a coverage-dependent kinetic model, which is distinct from that without coverage effects.[47] Considering the complexity of this issue, we discuss

preferentially the effect of other factors, such as functionals, the carbon deposition, the surface structure and the oxide support in the present work, before addressing it in a separate paper in the future.

Conclusions

DFT calculations and microkinetic studies are used to understand the discrepancy in the H-assisted CO activation mechanism during CO methanation at a low coverage regime. It was found that CHO is the preferred intermediate for C–O bond scission, followed by CH_2O on Co(0001), and this is different to the results of previous theoretical studies. The discrepancy can be explained by the lower energy path we identified for CHO decomposition, which mainly controls the rate of CO methanation. The dissociated O is removed preferentially by H_2O instead of by CO_2, formed through O hydrogenation, and is followed by OH disproportionation. The mechanism does not depend on the selection of functionals (SCAN, PBE and BEEF-vdW) and the presence of graphitic carbon, and likely also pertains to other Co surface structures, including some open facets and step sites. The roles of oxide supports and adsorbate–adsorbate interactions, which may account for the discrepancies between the theoretical studies on model Co surfaces and experimental studies on supported HCP Co catalysts, are also discussed. The work provides fundamental understanding of the mechanistic discrepancies in CO activation and methanation on HCP Co catalysts, and the insights obtained can be applied to other CO hydrogenation catalysts such as Ru-, Fe- and Ni-based catalysts.

Conflicts of interest

There are no conflicts to declare.

Acknowledgements

We are grateful for financial support from the National Natural Science Foundation of China (21872136, 21603146, 91645202, and 91945302), the Ministry of Science and Technology of China (2017YFA0204800 and 2017YFB0602205), the Guangdong Innovation Research Team for Higher Education (2017KCXTD030), the High-level Talents Project of Dongguan University of Technology (KCYKYQD2017017), the Guangdong Province Universities and Colleges Pearl River Scholar Funded Scheme (2019), the Guangdong Basic and Applied Basic Research Foundation (2019A1515011249) and the Key Research Project of Natural Science of Guangdong Provincial Department of Education (2019KZDXM010).

Notes and references

1 M. P. Andersson, F. Abild-Pedersen, I. N. Remediakis, T. Bligaard, G. Jones, J. Engbæk, O. Lytken, S. Horch, J. H. Nielsen, J. Sehested, J. R. Rostrup-Nielsen, J. K. Nørskov and I. Chorkendorff, *J. Catal.*, 2008, **255**, 6.

2 M. Kimura, T. Miyao, S. Komori, A. Chen, K. Higashiyama, H. Yamashita and M. Watanabe, *Appl. Catal., A*, 2010, **379**, 182.

3 H. Harms, B. Høhlein, E. Jørn and A. Skov, *Oil Gas J.*, 1980, **78**, 120.

4 M. Dry, *Appl. Catal., A*, 2004, **276**, 1; W. Gao, Q. S. Zhu and D. Ma, *Chin. J. Chem.*, 2018, **36**, 798.

5 S. Eckle, H.-G. Anfang and R. Jürgen Behm, *J. Phys. Chem. C*, 2011, **115**, 1361.

6 M. Ojeda, R. Nabar, A. U. Nilekar, A. Ishikawa, M. Mavrikakis and E. Iglesia, *J. Catal.*, 2010, **272**, 287; M. Ojeda, A. U. Li, R. Nabar, A. U. Nilekar, M. Mavrikakis and E. Iglesia, *J. Phys. Chem. C*, 2010, **114**, 19761.

7 J. Yang, Y. Y. Qi, J. Zhu, Y. A. Zhu, D. Chen and A. Holmen, *J. Catal.*, 2013, **308**, 37; Y. Y. Qi, J. Yang, X. Z. Duan, Y. A. Zhu, D. Chen and A. Holmen, *Catal. Sci. Technol.*, 2014, **4**, 3534.

8 A. Tuxen, S. Carenco, M. Chintapalli, C. H. Chuang, C. Escudero, E. Pach, P. Jiang, F. Borondics, B. Beberwyck, A. P. Alivisatos, G. Thornton, W. F. Pong, J. H. Guo, R. Perez, F. Besenbacher and M. Salmeron, *J. Am. Chem. Soc.*, 2013, **135**, 2273.

9 B. T. Loveless, C. Buda, M. Neurock and E. Iglesia, *J. Am. Chem. Soc.*, 2013, **135**, 6107.

10 J. J. C. Geerlings, M. C. Zonnevylle and C. P. M. de Groot, *Surf. Sci.*, 1991, **241**, 302; J. J. C. Geerlings, M. C. Zonnevylle and C. P. M. de Groot, *Surf. Sci.*, 1991, **241**, 315.

11 S. B. Vendelbo, M. Johansson, J. H. Nielsen and I. Chorkendorff, *Phys. Chem. Chem. Phys.*, 2011, **13**, 4486.

12 R. D. Kelley and D. Wayne Goodman, *Surf. Sci.*, 1982, **123**, L743.

13 X. S. Zhang, N. Rui, X. Y. Jia, X. Hu and C. J. Liu, *Chin. J. Catal.*, 2019, **40**, 495.

14 J. X. Liu, H. Y. Su and W. X. Li, *Catal. Today*, 2013, **215**, 36.

15 J. X. Liu, H. Y. Su, D. P. Sun, B. Y. Zhang and W. X. Li, *J. Am. Chem. Soc.*, 2013, **135**, 16284.

16 H. Y. Su, Y. H. Zhao, J. X. Liu, K. J. Sun and W. X. Li, *Catal. Sci. Technol.*, 2017, **7**, 2967.

17 J. X. Liu, B. Y. Zhang, P. P. Chen, H. Y. Su and W. X. Li, *J. Phys. Chem. C*, 2016, **120**, 24895.

18 I. M. Ciobica and R. A. van Santen, *J. Phys. Chem. B*, 2003, **107**, 3808.

19 O. R. Inderwildi, S. J. Jenkins and D. A. King, *J. Phys. Chem. C*, 2008, **112**, 1305.

20 M. K. Zhuo, K. F. Tan, A. Borgna and M. Saeys, *J. Phys. Chem. C*, 2009, **113**, 8357.

21 J. Cheng, P. Hu, P. Ellis, S. French, G. Kelly and C. Martin Lok, *J. Phys. Chem. C*, 2008, **112**, 9464.

22 Y. H. Zhao, K. J. Sun, X. F. Ma, J. X. Liu, D. P. Sun, H. Y. Su and W. X. Li, *Angew. Chem., Int. Ed.*, 2011, **50**, 5335; Y. H. Zhao, J. X. Liu, H. Y. Su, K. J. Sun and W. X. Li, *ChemCatChem*, 2014, **6**, 1755.

23 C. F. Huo, J. Ren, Y. W. Li, J. G. Wang and H. J. Jiao, *J. Catal.*, 2007, **249**, 174; D. B. Cao, Y. W. Li, J. G. Wang and H. J. Jiao, *J. Mol. Catal. A: Chem.*, 2011, **346**, 55.

24 I. Y. Zhang and X. Xu, *ChemPhysChem*, 2012, **13**, 1486.
25 J. P. Perdew, J. A. Chevary, S. H. Vosko, K. A. Jackson, M. R. Pederson, D. J. Singh and C. Fiolhais, *Phys. Rev. B: Condens. Matter Mater. Phys.*, 1992, **46**, 6671; J. A. White and D. M. Bird, *Phys. Rev. B: Condens. Matter Mater. Phys.*, 1994, **50**, 4954.
26 J. P. Perdew, K. Burke and M. Ernzerhof, *Phys. Rev. Lett.*, 1996, **77**, 3865.
27 P. P. Chen, B. Y. Zhang, X. K. Gu and W. X. Li, *Chin. J. Chem. Phys.*, 2019, **32**, 437.
28 O. Ducreux, J. Lynch, B. Rebours, M. Roy and P. Chaumette, *Stud. Surf. Sci. Catal.*, 1998, **119**, 125; D. J. Moodley, J. van de Loosdrecht, A. M. Saib, M. J. Overett, A. K. Datye and J. W. Niemantsverdriet, *Appl. Catal., A*, 2009, **354**, 102; G. A. Beitel, A. Laskov, H. Oosterbeek and E. W. Kuipers, *J. Phys. Chem.*, 1996, **100**, 12494.
29 J. W. Sun, A. Ruzsinszky and J. P. Perdew, *Phys. Rev. Lett.*, 2015, **115**, 036402.
30 J. Wellendorff, K. T. Lundgaard, A. Møgelhøj, V. Petzold, D. D. Landis, J. K. Nørskov, T. Bligaard and K. W. Jacobsen, *Phys. Rev. B: Condens. Matter Mater. Phys.*, 2012, **85**, 235149.
31 J. C. W. Swart, E. van Steen, I. M. Ciobica and R. A. van Santen, *Phys. Chem. Chem. Phys.*, 2009, **11**, 803.
32 D. J. Klinke II, S. Wilke and L. J. Broadbelt, *J. Catal.*, 1998, **178**, 540.
33 K. F. Tan, J. Xu, J. Chang, A. Borgna and M. Saeys, *J. Catal.*, 2010, **274**, 121.
34 G. Kresse and J. Furthmuller, *Phys. Rev. B: Condens. Matter Mater. Phys.*, 1996, **54**, 11169.
35 H. J. Monkhorst and J. D. Pack, *Phys. Rev. B: Solid State*, 1976, **13**, 5188.
36 K. J. Sun, Y. H. Zhao, H. Y. Su and W. X. Li, *Theor. Chem. Acc.*, 2012, **131**, 1118.
37 G. Henkelman and H. Jonsson, *J. Chem. Phys.*, 2000, **113**, 9978.
38 S. S. Wang, M. Z. Jian, H. Y. Su and W. X. Li, *Chin. J. Chem. Phys.*, 2018, **31**, 284.
39 J. P. den Breejen, P. B. Radstake, G. L. Bezemer, J. H. Bitter, V. Frøseth, A. Holmen and K. P. de Jong, *J. Am. Chem. Soc.*, 2009, **131**, 7197.
40 C. Stegelmann, A. Andreasen and C. T. Campbell, *J. Am. Chem. Soc.*, 2009, **131**, 8077.
41 M. G. Evans and M. Polanyi, *Trans. Faraday Soc.*, 1938, **34**, 0011.
42 I. A. W. Filot, R. A. van Santen and E. J. M. Hensen, *Angew. Chem., Int. Ed.*, 2014, **53**, 12746; S. Wilke, V. Natoli and M. H. Cohen, *J. Chem. Phys.*, 2000, **112**, 9986.
43 K. J. Sun, M. Kohyama, S. Tanaka and S. Takeda, *J. Phys. Chem. C*, 2014, **118**, 1611.
44 R. Prins, *Chem. Rev.*, 2012, **112**, 2714.
45 H. Papp, *Surf. Sci.*, 1983, **129**, 205; G. A. Beitel, A. Laskov, H. Oosterbeek and E. W. Kuipers, *J. Phys. Chem.*, 1996, **100**, 12494.
46 A. C. Lausche, A. J. Medford, T. S. Khan, Y. Xu, T. Bligaard, F. Abild-Pedersen, J. K. Nørskov and F. Studt, *J. Catal.*, 2013, **307**, 275.
47 Z. H. Yao, C. X. Guo, Y. Mao and P. Hu, *ACS Catal.*, 2019, **9**, 5957.
48 Z. Chen, H. Wang, N. Q. Su, S. Duan, T. H. Shen and X. Xu, *ACS Catal.*, 2018, **8**, 5816.
49 B. Zijlstra, R. J. P. Broos, W. Chen, H. Oosterbeek, I. A. W. Filot and E. J. M. Hensen, *ACS Catal.*, 2019, **9**, 7365.

